INTERNATIONAL JOURNAL OF PRECISION ENGINEERING AND MANUFACTURING-GREEN TECHNOLOGY Vol. 3, No. 1, pp. 35-39 JANUARY 2016 / 35
DOI: 10.1007/s40684-016-0005-7 ISSN 2288-6206 (Print) / ISSN 2198-0810 (Online)

Substrate-Dependent Growth of Nanothin Film Solid Oxide Fuel Cells toward Cost-Effective Nanostructuring

Sanghoon Ji[1], Jinsu Ha[2], Taehyun Park[3], Yusung Kim[3], Bongjun Koo[4], Young Beom Kim[4], Jihwan An[5,#], and Suk Won Cha[1,3,#]

1 Graduate School of Convergence Science and Technology, Seoul National University, 145, Gwanggyo-ro, Yeongtong-gu, Suwon-si, Gyeonggi-do, 16229, South Korea
2 Energy Laboratory, Samsung Electronics Co., Ltd., 130, Samsung-ro, Yeongtong-gu, Suwon-si, Gyeonggi-do, 16678, South Korea
3 Department of Mechanical and Aerospace Engineering, Seoul National University, 1, Gwanak-ro, Gwanak-gu, Seoul, 08826, South Korea
4 Department of Mechanical Convergence Engineering, Hanyang University, 222, Wangsimni-ro, Seongdong-gu, Seoul, 04763, South Korea
5 Manufacturing Systems and Design Engineering Programme, Seoul National University of Science and Technology, 232, Gongneung-ro, Nowon-gu, Seoul, 01811, South Korea
Corresponding Author / Email: swcha@snu.ac.kr, TEL: +82-2-880-8050, FAX: +82-2-880-1696

KEYWORDS: Nanostructuring, Nanoporous substrate, Thin film electrolyte, Solid oxide fuel cell

Nanothin and pinhole-free electrolyte-embedded solid oxide fuel cells (SOFCs) on nanothin bottom electrode catalyst-coated anodic aluminum oxide (AAO) substrates with 20 nm and 80 nm-sized nanopores are morphologically and electrochemically characterized to identify the substrate-dependent nanostructuring effects. Reliable electrolytes were fabricated through the application of a protective layer deposited by atomic layer deposition, whose microstructural distortion reduced as the electrolyte became thinner. At 450°C, the SOFC on the AAO substrate with 80 nm nanopores generated a higher peak power density by approximately 22% than the SOFC on the AAO substrate with 20 nm nanopores when the electrolyte and the bottom electrode catalyst are as thin as 300 nm and 50 nm, respectively.

Manuscript received: April 15, 2015 / Revised: August 26, 2015 / Accepted: December 2, 2015
This paper was presented at ISGMA2015

1. Introduction

The exhaustion of fossil fuels that can be collected from the earth is motivating the realization of renewable energy-based electricity generators.[1] Solid oxide fuel cells (SOFCs), which generally operate at high temperatures (above 800°C) to achieve low ion-conducting resistance through a ceramic electrolyte, are considered as a promising candidate for use in such generators due to their high energy conversion efficiency, pollution-free exhaust, and simple balance of plant parts.[2] However, the applicability of SOFCs in mobile devices capable of having a considerable influence on modern life is poor due to the material and systemic issues resulting from their excessively high operation temperatures. Although research on thin film electrolytes carried out over several decades has appreciably alleviated these issues, low-temperature SOFCs with a thin film electrolyte typically generate insufficient output power due to a shortage of electrode reaction sites and sluggish reaction kinetics at the electrode/electrolyte interfaces.[3-5] Recently, the nanostructuring of a nanothin film electrolyte with a two-dimensional triple phase boundary (TPB), the electrochemically active site where the electrolyte, the electrode, and the fuel mutually contact, was successfully demonstrated in a micro-electro-mechanical system (MEMS). This achievement showed a peak power density of as high as 1.3 W/cm^2 at 450°C.[6,7] Nevertheless, this nanostructuring methodology with high process complexity is disadvantageous in the aspect of cost-effectiveness, which presents the necessity of more economical methods for the nanostructuring of thin film electrolytes.[8]

The shape of thin films tends to be strongly dependent on the surface morphology of substrates. Furthermore, the degree of microstructural distortion, i.e., a degree that the microstructure of coating material deviates from the shape of the substrate, in thin films on non-flat substrates reduces as the thin films become thinner.[9] This phenomenon implies that the TPB length in porous substrate-supported thin film SOFCs with a two-dimensional TPB can become longer if sufficiently thin components are coated on the substrate with a rough surface morphology. However, in most porous substrate-supported thin film SOFCs, the thicknesses of the electrolyte and the bottom electrode catalyst were too thick to manifest the effect of augmentation of TPB length through substrate-dependent growth.[1,3]

In this study, the nanostructuring effects of a 'nanothin and pinhole-free electrolyte' and a nanothin bottom electrode catalyst on a porous

substrate with different-sized nanopores are investigated in terms of microstructure and electrochemical performance. In particular, a nanothin and pinhole-fee electrolyte deposited by atomic layer deposition (ALD) was inserted between sputtered bi-layer electrolyte layers with high functionality.[10,11] We demonstrated that the nanostructuring by substrate morphology becomes more prevalent with larger nanopores and therefore ensures larger electrolyte surface area, which appreciably enhances the cell performance due to the faster reaction kinetics on the cathode side.

2. Experimental Methods

2.1 Thin Film Fabrication

For the deposition of the electrolyte, yttria-stabilized zirconia (YSZ) thin film was deposited using a commercial sputtering machine (A-Tech System, South Korea) equipped with a customized rotation unit. The target-to-substrate distance was set to 75 nm, and the substrate support was rotated at 4 rpm to assure the uniform growth rate in the lateral direction. A mixture of Ar and O_2 at a volumetric ratio of 80:20 was used for the sputtering gas. The base pressure was maintained at approximately 1.0×10^{-4} Pa; the background pressure was kept at 1.3 Pa during the deposition step. The radio-frequency magnetron power of the sputtering gun was adjusted to 50 W, and an YSZ disk pellet with 8 mol% of Y_2O_3 was used as the target. Sputtered gadolinium-doped ceria (GDC) thin films were deposited under the same processing conditions with a GDC disk pellet with 10 mol % of Gd_2O_3. The fabrication process of ALD-deposited YSZ ultra-thin film used as the electrolyte protective layer is presented in our previous work.[12] The growth rate of ALD YSZ on sputtered YSZ film was -1.0 Å/cycle. For the deposition of the electrode, a 99.99% pure Pt target was used to deposit Pt thin films with 200 W of direct current (DC) power in a 99.9999% pure Ar atmosphere. The background pressure was kept at 0.7 Pa and 12 Pa for the dense and porous microstructures, respectively.

2.2 Thin Film Characterization

The quantitative analysis of surface morphology was examined by atomic force microscopy (AFM) using an XE 100 (Park Systems, South Korea) instrument. The tapping mode AFM scanning herein was carried out using silicon tips with a radius of -20 nm at a scan rate of 0.4 Hz. The qualitative analysis of surface morphology was analyzed by field emission scanning electron microscopy (FE-SEM) using a Quanta 3D FEG (FEI Company, Netherland) instrument at an acceleration voltage of 5 kV, in which every sample was coated with sub-5 nm-thick Pt to diminish the surface discharge.

2.3 Electrochemical Evaluation

100 micrometer-thick commercial anodic aluminum oxide (AAO, Synkera, USA) templates consisting of Al foil anodized in an acid solution to form well-arrayed nanopores with pore sizes of 20 nm (hereafter called “AAO-20”) and 80 nm (hereafter called “AAO-80”) were used as the porous supporter for fabricated thin film SOFCs.[13] The physical mask for the opening area 1 mm^2 in size consisted of a square-patterned 0.1 mm-thick stainless steel (SS) plate (lower part) and a much thicker SS plate pressing the lower plate (upper part). Test cells were attached to a custom-made H_2 feeding chamber using a ceramic adhesive (CP4010, Aremco Products, USA). They were heated to 450°C at a ramping rate of 10°C/min using high-capacity halogen lamps. 50 sccm of dry H_2 gas was supplied to the anode side, and the cathode was exposed to the atmospheric environment. The anode was connected with a combination of Ag paste (597A, Aremco Products, USA) and a 0.5 mm diameter Ag wire, while the cathode was directly contacted using a probe of hardened-steel with a radius of 0.19 mm moved by a XYZ stage. Polarization curve measurements and electrochemical impedance spectroscopy (EIS) analysis of the test cells were taken using an electrochemical testing system (1287/1260, Solatron Analytical, UK). During the EIS analysis, the alternating voltage with amplitude of 50 mV and the DC bias voltage of 0.1 V were applied to the cathode with respect to the anode.

3. Results and Discussion

AAO substrates with different-sized nanopores are used for the nanostructuring of thin film electrolytes, whose surface morphologies are examined from local height profiles extracted from AFM topographical data (Fig. 1).[14] The surface morphology of the AAO substrates is roughly distinguishable by the distribution of the flexures shown in the height profiles. The approximate maximum height difference (vertical distance from the top to the bottom) of AAO-80 is approximately 3.3 fold higher than that of the AAO-20. This difference is most likely due to the differences in the sizes of the AAO nanopores.

Four types of cells were fabricated to investigate the effects of the substrate shape and the electrolyte thickness on the electrochemical performance, as shown in the schematic diagram in Fig. 2(a). AAO-20’s were used for Cell-1 and Cell-3, and AAO-80’s were used for Cell-2 and Cell-4, respectively. Thin film electrolytes with total thickness of 600 nm (YSZ: 100 nm, GDC: 500 nm) were used for Cell-1 and Cell-2, and those with 300 nm (YSZ: 100 nm, GDC: 200 nm) were used for Cell-3 and Cell-4, respectively. In this process, Pt bottom electrode catalyst as thin as 50 nm used as the anode is initially deposited on the AAO substrate to mitigate the degree of

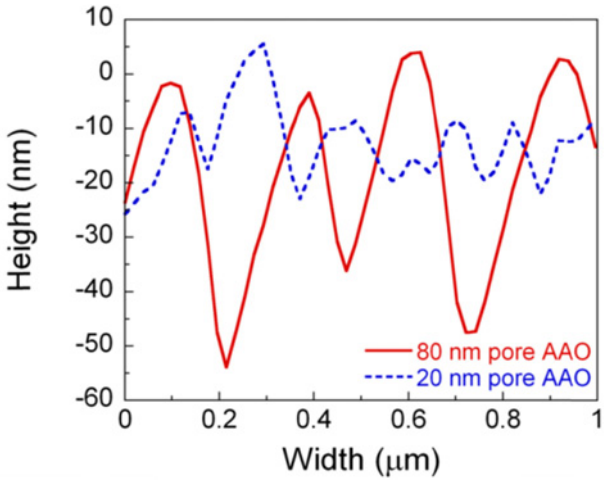

Fig. 1 Atomic force microscopy height profiling of anodic aluminum oxide (AAO) substrates with 20 nm and 80 nm-sized nanopores

morphological distortion of the substrate shape. Prior to the deposition of ALD YSZ, which serves as an electrolyte protective layer, 50 nm-thick sputtered YSZ with relatively low step coverage is deposited onto the Pt/AAO substrates to prevent the Pt bottom electrode catalyst from being blanked by the ALD YSZ.[15] The thickness of the ALD YSZ protective layer is adjusted to 50 nm which is sufficient to block a few nanometers of the pinholes existing in the sputtered YSZ considering the grain size of typical ALD YSZ films.[16] The surface morphologies of the ALD YSZ deposited onto the sputtered-YSZ/Pt/AAO-20 and sputtered-YSZ/Pt/AAO-80 samples are noticeably different, as shown in Fig. 2(b). Sputtered- YSZ/Pt/AAO-80 platform, in particular, leads to the formation of a very rough surface of the ALD YSZ whose AFM root mean square roughness is approximately 120 nm. GDC is then deposited onto the ALD YSZ protective layers to accelerate the oxygen reduction reaction kinetics which is well known as the most sluggish reaction step and therefore results in poor electrochemical performance of low-temperature SOFCs.[17] Finally, a Pt top electrode catalyst of 50 nm thickness, which is used as the cathode, is deposited on the top of the multi-layer electrolyte layers. The open-circuit voltages of all cells range from 1.13 V to 1.16 V, which resultantly indicates that the degree of performance deterioration originating from pinholes effects through the electrolyte is negligible.[18] Fig. 2(c) shows the peak power density and the electrolyte thickness of the four cells. The peak power density of Cell-1 is slightly higher than that of Cell-2. Based on the fact that the surface morphologies of the electrolytes with two cells as confirmed in FE-SEM images are nearly identical, it is considered that this difference in the peak power density is caused by the difference in TPB lengths on the anode side; Cell-1 has far higher nanopore density and, therefore, larger TPB density at the anode than Cell-2. Cell-3 and Cell-4, which have 50% thinner electrolytes than Cell-1 and Cell-2, produce higher peak power densities than Cell-1 and Cell-2 due to reduced ohmic resistance.[17]

Interestingly, among the cells with thinner (300 nm) electrolytes, the peak power of Cell-4 is much higher than that of Cell-3. Polarization curve measurements and EIS analysis were conducted for Cell-3 and

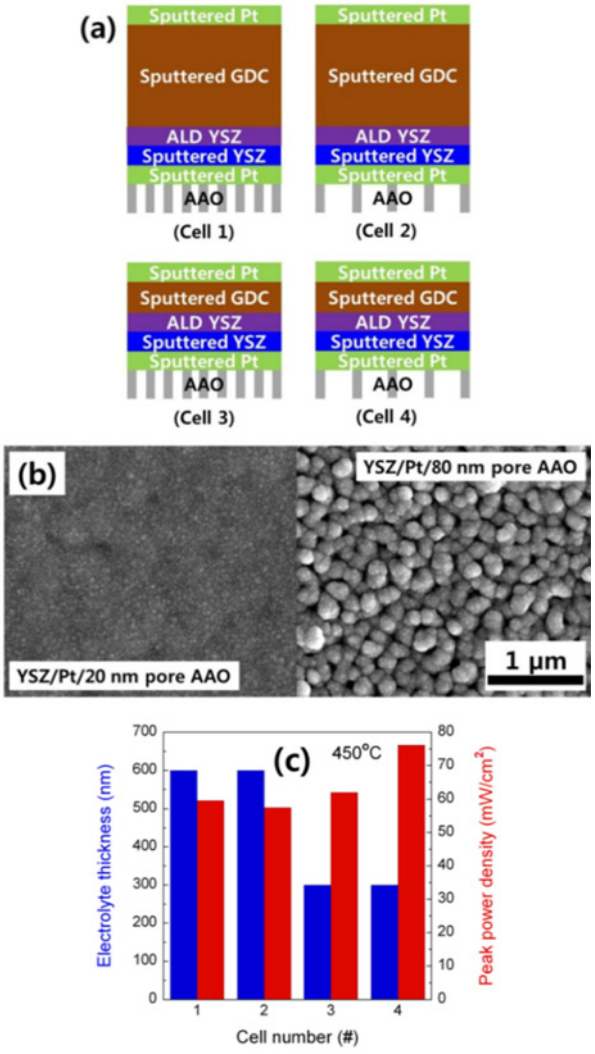

Fig. 2 (a) Schematic structures of four yttria-stabilized zirconia (YSZ)/ gadolinium-doped ceria (GDC) electrolyte cells with different kinds of the substrate type and electrolyte thickness (b) Field emission scanning electron microscopy (FE-SEM) top-view images of 100 nm-thick YSZ deposited on the 50 nm Pt-coated AAO with different-sized nanopores (20 nm and 80 nm) (c) Electrolyte thicknesses and peak power densities of the four cells

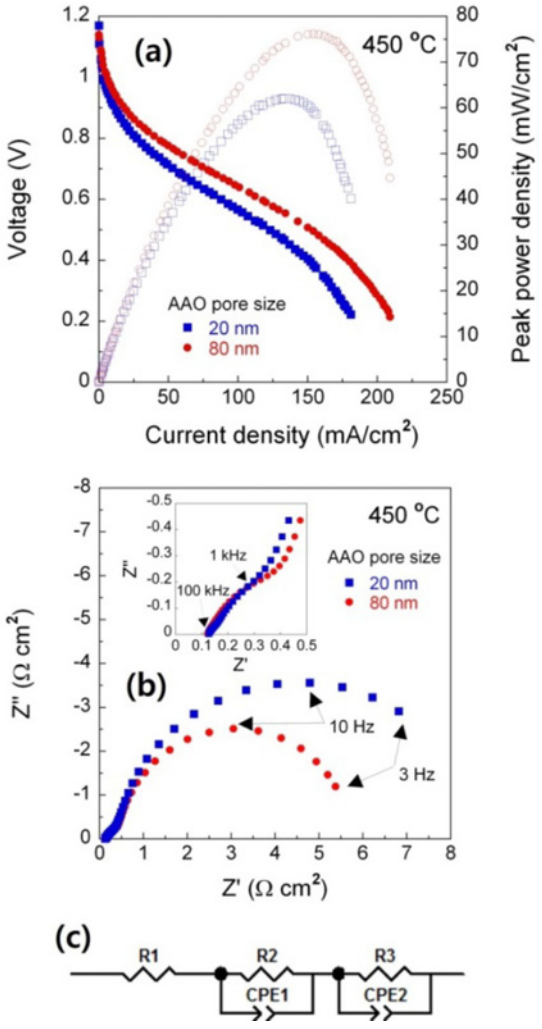

Fig. 3 (a) Polarization curves of 300 nm-thick electrolyte cells on AAO substrates with different-sized nanopores (20 nm and 80 nm) at 450°C (b) Their electrochemical impedance spectroscopy (EIS) analysis results at 450°C (c) An equivalent circuit for EIS data interpretation

Cell-4 to verify the contribution of individual resistances. As shown in Fig. 3(a), a voltage drop appearing at a low current density regime (below 10 mA/cm^2), an approximate indicator used to estimate the amount of activation loss, reveals that Cell-3 with 80 nm-sized nanopores has less activation overpotential compared to Cell-4 with 20 nm-sized nanopores.[18,19] EIS analysis results show that there is a significant difference in the arc size between the two cells. The lack of overlapping of the arcs under various bias voltages indicates that all arcs are relevant to the reaction kinetics at the electrode-electrolyte interfaces (not shown in the figure).[20,21] There are two remarkable arcs with time constants of 1 kHz and 10 Hz (Fig. 3(b)). The individual resistances of the cells are estimated by a non-linear square-fitting algorithm for the selected equivalent circuit shown in Fig. 3(c). According to the general concept of EIS interpretations, two arcs drawn in higher and lower frequency regimes are considered as the anode and cathode resistances, respectively.[17,18] The anode-electrolyte interfacial resistance of Cell-4 is slightly higher than that of Cell-3; in contrast, the cathode-electrolyte interfacial resistance of Cell-4 is much lower than that of Cell-3. This analysis result presents that the TPB length on the cathode side of Cell-4 may be longer than that of Cell-3, as was confirmed by FE-SEM top-view images showing that the electrolyte surface morphology of Cell-4 is much rougher than that of Cell-3 (Fig. 4).

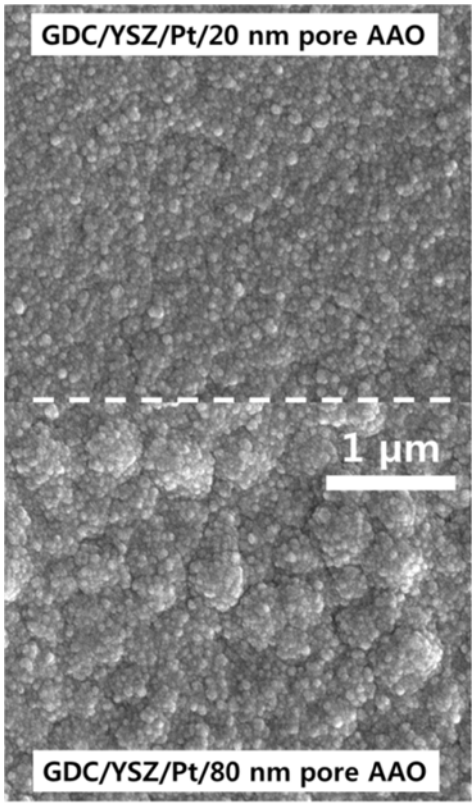

Fig. 4 FE-SEM top-view images of 200 nm-thick GDC on 100 nm-thick YSZ and 50 nm-thick Pt-coated AAO substrates with different-sized nanopores (20 nm and 80 nm)

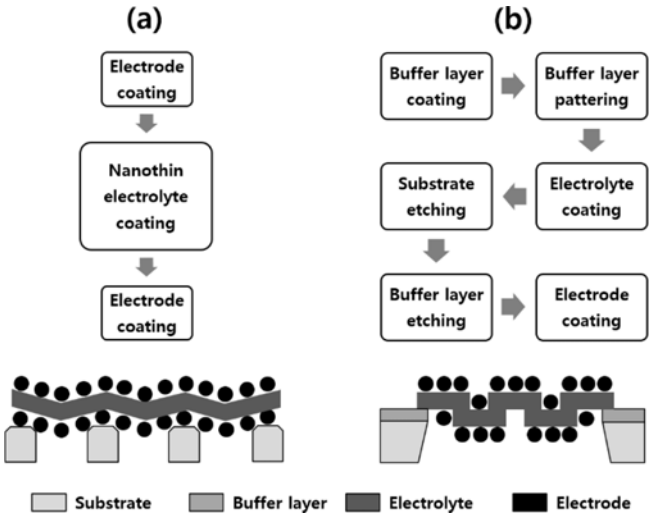

Fig. 5 Comparison between (on the left) self-nanostructuring method through use of a nanoporous substrate, a nanothin bottom electrode catalyst, and a nanothin film electrolyte and (on the right) common nanostructuring method based on micro-electro-mechanical system technologies, in terms of process

Compared to the nanostructuring methodology investigated in this study (as shown on the left side of Fig. 5), common nanostructuring methodologies of thin film electrolyte for SOFCs have low productivity levels due to their relatively high number of procedures (as shown on the right side of Fig. 5). Explicitly, this fact indicates that nanostructuring methodology suggested in this study has a strength over common nanostructuring methodologies such as MEMS from the productivity perspective. Nevertheless, because the fabrication of nanothin and dense electrolytes generally necessitates the use of costly coating techniques such as ALD, the application of the substrate-dependent nanostructuring process with nanoporous substrates may have larger practical implications when it is combined with economic coating techniques.[16]

4. Conclusions

We confirmed that a 'nanothin and pinhole-free' electrolyte and a nanothin bottom electrode catalyst on a nanoporous ceramic substrate can lead to substrate-dependent nanostructuring for high-performance low-temperature SOFCs. When a 300 nm-thick electrolyte film with a 50 nm-thick ALD YSZ protective layer is employed, for instance, the peak power density of the thin film SOFC on an AAO substrate with 80 nm-sized nanopores is approximately 22% higher than that of the thin film SOFC on an AAO substrate with 20 nm-sized nanopores at 450°C. However, such a performance enhancement due to nanostructuring by rough substrate surface was not shown in the cells with thicker electrolytes. We consequently think that the substrate-dependent nanostructuring technique may have great potentials as an economical nanostructuring methodology for nanoscale electrochemical devices compared to the existing MEMS-based techniques.

ACKNOWLEDGEMENT

This work was supported by the Global Frontier R&D Program on Center for Multiscale Energy System funded by the National Research

Foundation under the Ministry of Science, ICT & Future Planning, Korea (2015M3A6A7065442). In addition, Jihwan An acknowledges partial support from the National Research Foundation of Korea (NRF) grant funded by the Korea government (NRF-2015R1D1A1A01058963).

REFERENCES

1. Son, J.-W. and Song, H.-S., "Influence of Current Collector and Cathode Area Discrepancy on Performance Evaluation of Solid Oxide Fuel Cell with Thin-Film-Processed Cathode," Int. J. Precis. Eng. Manuf.-Green Tech., Vol. 1, No. 4, pp. 313-316, 2014.
2. Choi, H., Cho, G. Y., and Cha, S.-W., "Fabrication and Characterization of Anode Supported YSZ/GDC Bilayer Electrolyte SOFC Using Dry Press Process," Int. J. Precis. Eng. Manuf.-Green Tech., Vol. 1, No. 2, pp. 95-99, 2014.
3. Ji, S., Chang, I., Lee, Y. H., Lee, M. H., and Cha, S. W., "Performance Enhancement of Thin-Film Ceramic Electrolyte Fuel Cell Using Bi-Layered Yttrium-Doped Barium Zirconate," Thin Solid Films, Vol. 539, pp. 117-121, 2013.
4. Lee, W. and Prinz, F. B., "Localized Charge Transfer Reactions near the Pt-YSZ Interfaces Using Kelvin Probe Microscopy," Int. J. Precis. Eng. Manuf.-Green Tech., Vol. 1, No. 3, pp. 201-205, 2014.
5. Pornprasertsuk, R., Yuwapattanawong, C., Permkittikul, S., and Tungtidtham, T., "Preparation of Doped $BaZrO_3$ and $BaCeO_3$ from Nanopowders," Int. J. Precis. Eng. Manuf., Vol. 13, No. 10, pp. 1813-1819, 2012.
6. An, J., Kim, Y.-B., Park, J., Gur, T. M., and Prinz, F. B., "Three-Dimensional Nanostructured Bilayer Solid Oxide Fuel Cell with 1.3 W/cm^2 at 450 °C," Nano letters, Vol. 13, No. 9, pp. 4551-4555, 2013.
7. An, J., Kim, Y. B., Jung, H. J., Park, J. S., Cha, S. W., et al., "Structural and Compositional Analysis of Solid Oxide Fuel Cell Electrolytes Using Transmission Electron Microscopy," Int. J. Precis. Eng. Manuf., Vol. 13, No. 7, pp. 1273-1279, 2012.
8. Su, P.-C. and Prinz, F. B., "Nanoscale Membrane Electrolyte Array for Solid Oxide Fuel Cells," Electrochemistry Communications, Vol. 16, No. 1, pp. 77-79, 2012.
9. Thirumalairajan, S., Girija, K., Mastelaro, V. R., and Ponpandian, N., "Surface Morphology-Dependent Room-Temperature $LaFeO_3$ Nanostructure Thin Films as Selective NO_2 Gas Sensor Prepared by Radio Frequency Magnetron Sputtering," ACS Applied Materials and Interfaces, Vol. 6, No. 16, pp. 13917-13927, 2014.
10. Cassir, M., Ringuedé, A, and Niinistö, L., "Input of Atomic Layer Deposition for Solid Oxide Fuel Cell Applications," Journal of Materials Chemistry, Vol. 20, No. 41, pp. 8987-8993, 2010.
11. Bachmann, J., "Atomic Layer Deposition, a Unique Method for the Preparation of Energy Conversion Devices," Beilstein Journal of Nanotechnology, Vol. 5, No. 1, pp. 245-248, 2014.
12. Ji, S., Chang, I., Lee, Y. H., Park, J., Paek, J. Y., et al., "Fabrication of Low-Temperature Solid Oxide Fuel Cells with a Nanothin Protective Layer by Atomic Layer Deposition," Nanoscale Research Letters, Vol. 8, Paper No. 48, 2013.
13. Kim, M., Ha, Y.-C., Nguyen, T. N., Choi, H. Y., and Kim, D., "Extended Self-Ordering Regime in Hard Anodization and Its Application to Make Asymmetric AAO Membranes for Large Pitch-Distance Nanostructures," Nanotechnology, Vol. 24, No. 50, Paper No. 505304, 2013.
14. Lee, M. H. and Hwang, C. S., "Resistive Switching Memory: Observations with Scanning Probe Microscopy," Nanoscale, Vol. 3, No. 2, pp. 490-502, 2011.
15. Kwon, C.-W., Son, J.-W., Lee, J.-H., Kim, H.-M., Lee, H.-W., et al., "High-Performance Micro-Solid Oxide Fuel Cells Fabricated on Nanoporous Anodic Aluminum Oxide Templates," Advanced Functional Materials, Vol. 21, No. 6, pp. 1154-1159, 2011.
16. Shim, J. H., Kang, S., Cha, S-.W., Lee, W., Kim, Y. B., et al., "Atomic Layer Deposition of Thin-Film Ceramic Electrolytes for High-Performance Fuel Cells," Journal of Materials Chemistry: A, Vol. 1, No. 41, pp. 12695-12705, 2013.
17. Ji, S., Cho, G. Y., Yu, W., Su, P.-C., Lee, M. H., et al., "Plasma-Enhanced Atomic Layer Deposition of Nanoscale Yttria-Stabilized Zirconia Electrolyte for Solid Oxide Fuel Cells with Porous Substrate," ACS Applied Materials and Interfaces, Vol. 7, No. 5, pp. 2998-3002, 2015.
18. Ji, S., Chang, I., Cho, G. Y., Lee, Y. H., Shim, J. H., et al., "Application of Dense Nano-Thin Platinum Films for Low-Temperature Solid Oxide Fuel Cells by Atomic Layer Deposition," International Journal of Hydrogen Energy, Vol. 39, No. 23, pp. 12402-12408, 2014.
19. Ji, S., Hwang, Y.-S., Park, T., Lee, Y. H., Peak, J. Y., et al., "Graphite Foil Based Assembled Bipolar Plates for Polymer Electrolyte Fuel Cells," Int. J. Precis. Eng. Manuf., Vol. 13, No. 12, pp. 2183-2186, 2012.
20. Ji, S., Lee, Y. H., Park, T., Cho, G. Y., Noh, S., et al., "Doped Ceria Anode Interlayer for Low-Temperature Solid Oxide Fuel Cells with Nanothin Electrolyte," Thin Solid Films, Vol. 591, pp. 250-254, 2015.
21. Ji, S., Tanveer, W. H., Yu, W., Kang, S., Cho, G. Y., et al., "Surface Engineering of Nanoporous Substrate for Solid Oxide Fuel Cells with Atomic Layer-Deposited Electrolyte," Beilstein Journal of Nanotechnology, Vol. 6, No. 1, pp. 1805-1810, 2015.